Matter and Radiation at Extremes | RESEARCH ARTICLE | scitation.org/journal/mre

Generating optical supercontinuum and frequency comb in tenuous plasmas

Cite as: Matter Radiat. Extremes 6, 054402 (2021); doi: 10.1063/5.0052829
Submitted: 1 April 2021 • Accepted: 10 July 2021 •
Published Online: 5 August 2021

View Online Export Citation CrossMark

Kenan Qu[a] and Nathaniel J. Fisch

AFFILIATIONS

Department of Astrophysical Sciences, Princeton University, Princeton, New Jersey 08544, USA

Note: This paper is a part of the Special Topic Collection on Plasma Optics.
[a]**Author to whom correspondence should be addressed:** kq@princeton.edu

ABSTRACT

There are several mechanisms by which the frequency spectrum of a laser broadens when it propagates at near-relativistic intensity in a tenuous plasma. Focusing on one-dimensional effects, we identify two strong optical nonlinearities, namely, four-wave mixing (FWM) and forward Raman scattering (FRS), for creating octave-wide spectra. FWM dominates the interaction when the laser pulse is short and intense, and its combination with phase modulation produces a symmetrically broadened supercontinuum. FRS dominates when the laser pulse is long and relatively weak, and it broadens the laser spectrum mainly toward lower frequencies and produces a frequency comb. The frequency chirping combined with group velocity dispersion compresses the laser pulse, causing higher peak intensity.

I. INTRODUCTION

Wideband laser spectra[1–3] with high intensities are capable of overcoming plasma instabilities, such as Raman/Brillouin scattering[4–10] and filamentation,[5,6] and enable efficient laser power delivery.[11–13] Numerical simulations show that they can propagate over an extended distance through plasmas without incurring significant pulse distortion[14–16] or absorption.[11,17,18] Hence, they are useful in numerous laser–plasma applications, such as laser–plasma accelerators,[19] inertial confinement fusion,[13,20] and extreme ultraviolet (EUV) radiation.[21] However, traditional methods using nonlinear optical crystals cannot efficiently produce wideband spectra at high power.[22,23]

Actually, plasmas can be used to broaden the laser spectrum because of their strong optical nonlinear susceptibility and high thermal resistance. It has been theoretically proposed[24–30] that the spectrum of a dual-color continuous laser wave can be broadened in a plasma through cascades of forward Raman scattering (FRS).[26,27] The plasma electron waves couple laser components that are detuned by the plasma frequency. Hence, a pair of continuous lasers can be converted into a wideband spectrum with discrete spikes, i.e., an optical frequency comb.[31–34] If one of the laser pulses is at relativistic intensity ($\gtrsim 10^{18}$ W cm^{-2} at ~ 1 μm wavelength), a frequency comb could also be generated in the plasma wakefield.[35]

In this paper, we revisit the cascaded broadening of the laser spectrum in plasmas and point out a new regime dominated by four-wave mixing (FWM).[36–39] The FWM-dominated process produces a wideband continuous spectrum without discreteness, i.e., an optical supercontinuum.[40,41] We compare the FWM and FRS processes to show that the cascade generates a supercontinuum when the laser pulse is short relative to a few plasma wave periods and has near-relativistic intensity, and otherwise it generates a frequency comb. The combination of short pulse duration and high intensity cause strong phase modulation and chirping. It flattens each frequency sideband and creates a continuous spectrum. Given sufficient plasma length, either the supercontinuum or frequency comb can reach almost a full electromagnetic spectrum spanning multiple octaves.

To create the wideband spectrum, a pair of copropagating laser pulses with detuning of the plasma frequency is sent into a plasma. They beat to create a plasma Langmuir wave[24,25] if FRS dominates, or an electron mass perturbation (a virtual phonon) if FWM dominates. Both the plasma wave and the virtual phonon scatter the laser and broaden the spectrum at multiples of the plasma frequency. From a quantum point of view, a photon can either split into a lower-frequency photon and a phonon/virtual phonon or convert itself into a higher-frequency photon by combining with a phonon/virtual phonon. Since the frequency downconversion process takes place at a higher interaction rate, the phonon/virtual phonon number grows and the spectrum expands. The process can terminate owing to wavevector mismatch near the plasma frequency before exiting the plasma medium.

The plasma wave excited through FRS has a phase velocity near the speed of light, but no group velocity. Zero group velocity means that the plasma wave propagates backward in the laser frame, causing energy transport from the laser front to the tail. The growing plasma wave amplitude leads to a wider spectrum in the laser pulse tail than the front. Owing to the energy consumption by the plasma wave, the laser spectrum shows an overall frequency downshift.

FWM is a parametric process that does not excite a plasma wave and thus conserves the total electromagnetic energy. The virtual phonon amplitude does not grow or decay and is determined solely by the instantaneous laser waves. Hence, the virtual phonon has its maximum amplitude at the laser peak, where the greatest spectral broadening takes place. With conserved laser energy and photon number, the spectrum is broadened symmetrically besides the input laser frequency. The short pulse duration and high intensity combine to produce a strong chirp to stretch each frequency sideband and form a supercontinuum.

This paper focuses on one-dimensional (1D) laser pulse evolution to compare the FWM and FRS processes. It is organized as follows. In Sec. II, we model the laser propagation problem and explain the laser nonlinearities. In Sec. III, we identify two different interaction regimes dominated by FRS and FWM, respectively, and find the growth of the plasma wave and virtual phonon. In Sec. IV, we find the scaling laws of the frequency bandwidth in each regime. In Sec. V, we analyze the temporal envelope evolution of the laser pulse. In Sec. VI, using particle-in-cell (PIC) simulations, we demonstrate the generation of a supercontinuum and a frequency comb. In Sec. VII, we present our conclusions.

II. MODEL

We consider a cold plasma that responds to the laser field only through the electromagnetic potentials and relativistic effects. The laser pulse evolution is described by the coupled laser–plasma equations in the 1D form[6,19]

$$(\partial_{tt}-c^2\partial_{zz})a=\frac{\omega_p^2}{\gamma}\frac{n}{\bar{n}}a\cong\omega_p^2\left(1+\tilde{n}-\frac{a^2}{2}\right)a, \tag{1}$$

$$(\partial_{tt}+2\nu\omega_p+\omega_p^2)\tilde{n}=\frac{c^2}{2}\partial_{zz}a^2, \tag{2}$$

where a is the dimensionless vector potential normalized to the laser intensity I as $I[\mathrm{W\,cm^{-2}}]=1.37\times10^{18}(a/\lambda[\mu\mathrm{m}])^2$, $\gamma=\sqrt{1+a^2}$ is the Lorentz factor of the electrons, $\tilde{n}=(n-\bar{n})/\bar{n}$ is the normalized perturbed electron density, and n and $\bar{n}$ are the local and average electron densities, respectively. c is the speed of light in vacuum and ω_p is plasma frequency at density $\bar{n}$. The expansion in Eq. (1) is valid for $\tilde{n}\ll1$ and $a\ll1$. We include a heuristic damping factor ν in Eq. (2) to describe plasma wave damping. Our discussion focuses on laser pulses with duration longer than or comparable to a plasma wavelength to avoid wakefield excitation.

The nonlinear term proportional to a^3 accounts for the change in mass when the electrons are driven to near-relativistic velocity in the strong laser field. Its coefficient, $-\omega_p^2/2$, results from the first-order expansion of $\omega_p^2/\gamma=\omega_p^2/\sqrt{1+a^2}\approx\omega_p^2(1-a^2/2)$. The change in plasma frequency can, in turn, modulate the laser field. This instantaneous mutual coupling between the laser field and the electrostatic potential is investigated in a more general formalism in Ref. 38. It is found that the plasma-to-laser back-action yields a correction term $(\omega_p^2/2)c^2\partial_{zz}(\partial_t^2+\omega_p^2)^{-1}$ in addition to the nonlinear coefficient, $-\omega_p^2/2$. The correction term is nevertheless very small in tenuous plasmas, and we neglect it in the rest of this article. We will present PIC simulations in Sec. VI to justify the use of Eqs. (1) and (2).

The plasma wave is most strongly excited at its eigenfrequency ω_p, which scatters the laser wave into discrete frequencies. We therefore expand the laser field and plasma density perturbation as

$$a=\sum_j a_j e^{-i\omega_j t+ik_j z}+\text{c.c.}, \tag{3}$$

$$\tilde{n}=\delta n e^{-i\omega_p t+ik_p z}+\text{c.c.}, \tag{4}$$

where $\omega_j=\omega_0+j\omega_p>0$, $k_j=k_0+jk_p>0$, and $\omega_0(k_0)$ is the frequency (wavenumber) of the pump laser. It is worth noting that plasma density perturbations could also exhibit higher harmonics in the Langmuir wave-breaking limit[42,43] or even below this limit if the plasma has finite temperature.[44] We refrain from considering these effects, since we work with very low plasma density at zero temperature.

In the low-plasma-density limit $\omega_j\gg\omega_p$, the dispersion relation $\omega_j^2=c^2k_j^2+\omega_p^2$ is approximated as $\omega_j\approx ck_j$, and so $\omega_p\approx ck_p$. Matching the fast-oscillation components in Eqs. (1) and (2) yields

$$(\partial_t+v_{g,j}\partial_z)a_j=-\frac{\omega_p^2}{2i\omega_j}(\delta n^* a_{j+1}+\delta n a_{j-1})+\frac{3\omega_p^2}{4i\omega_j}\times\left[\sum_k|a_k|^2a_j+\sum_{m,n}^{m\neq n}a_m^*a_n a_{m-n+j}+\text{TSFG}\right], \tag{5}$$

$$(\partial_t+i\nu)\delta n=-\frac{\omega_p}{2i}\sum_j a_{j+1}a_j^*, \tag{6}$$

where $v_{g,j}=c^2k_j/\omega_j$ is the group velocity of frequency component ω_j. The first term on the right-hand side of Eq. (5) describes the laser anti-Stokes and Stokes Raman scattering by the plasma wave. A photon is created either by annihilation of an anti-Stokes photon and creation of a phonon or by annihilation of both a Stokes photon and a phonon, as illustrated in Fig. 1(a). Inside the square brackets are the terms for phase modulation (including self-phase modulation for $k=j$ and cross-phase modulation for $k\neq j$), FWM, and third-order sum-frequency generation (TSFG), respectively. The phase modulation nonlinearity only induces a phase shift, without causing energy dissipation or redistribution. The FWM nonlinearity describes the annihilation of two photons to create two new photons at different frequencies, as illustrated in Fig. 1(b). The FWM nonlinearity can create photons at new frequencies, similar to the FRS process, without

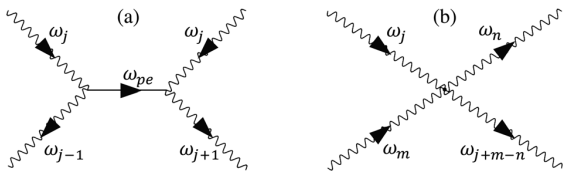

FIG. 1. Diagrams of (a) FRS and (b) FWM processes.

exciting plasma waves. Each FWM stage is similar to the process discussed in Ref. 39 in the absence of nonlinear resonance broadening effects. The TSFG nonlinearity describes combination of three photons and creation of a photon at the three-photon-sum frequency. The four photons in TSFG have dramatically different frequencies, making it difficult to satisfy the phase matching condition. Hence, we neglect the TSFG term in the following discussion. Equation (6) describes the plasma wave amplitude driven by the beat of two adjacent electromagnetic sidebands. A phonon is created when a photon is converted into a Stokes photon.

For spatial–temporal analysis, we next introduce a coordinate system that is comoving with the speed of light: $\zeta = t - z/c$ and $\tau = z/c$. Equations (5) and (6) are then transformed into

$$\left[\partial_\tau + \left(\frac{c}{v_{g,j}} - 1\right)\partial_\zeta\right] a_j = -\frac{\omega_p^2}{2ick_j}\left(\delta n^* a_{j+1} + \delta n a_{j-1}\right) + \frac{3\omega_p^2}{4ick_j}\sum_l \chi_l a_{j-l}, \tag{7}$$

$$(\partial_\zeta + i\nu)\delta n = -\frac{\omega_p}{2i}\sum_j a_{j+1}a_j^*, \tag{8}$$

$$\chi_l = \sum_j a_{j+l}a_j^*. \tag{9}$$

Here, we have introduced the virtual phonon parameter χ_l to describe the phase modulation nonlinearity for $l = 0$ and the FWM nonlinearity for $l \neq 0$. It obeys the relation $\chi_l^* = \chi_{-l}$. Note that the virtual phonon is not a wave, and so it does not propagate or decay.

Although the phase modulation process does not generate new discrete frequency sidebands, it flattens each sideband by inducing a chirp. For short laser pulses, the phase modulation, which is proportional to $\chi_0(\tau, \zeta)$, varies rapidly within the pulse duration. It broadens the spectrum by an amount $[\omega_p^2\tau/(2\omega_j)](\partial_\zeta\chi_0)$. We will show in Sec. III C that χ_0 remains quasi-constant during the interaction. Each sideband thus expands linearly with τ, and eventually merges with adjacent sidebands when it broadens to ω_p. For an input pulse with duration T and a peak value χ_{0M}, the spectrum loses discreteness and becomes a supercontinuum when

$$\omega_p\tau \gtrsim \frac{T\omega_j}{\chi_{0M}}. \tag{10}$$

III. TWO REGIMES OF OPERATION: FWM AND FRS

Each new frequency component is created when an existing photon combines with a phonon or a virtual phonon. Starting with a pump photon a_o and a probe photon a_{o-1} at adjacent frequencies, FWM directly creates the anti-Stokes sideband a_{o+1} and the Stokes sideband a_{o-2} via the instantaneous virtual phonon. The pump and probe waves also excite a plasma wave δn whose amplitude increases along ζ. The plasma wave then combines with the pump and probe photon to contribute to a_{o+1} and a_{o-2}. But the mediating plasma wave δn introduces a $\pi/2$ phase, and hence the two paths of creation of the new sidebands do not coherently add to each other.

FRS and FWM scatter the laser in distinctive manners. *First*, the plasma wave amplitude grows in the direction ζ, but the virtual phonon amplitude is determined solely by the instantaneous laser field. Consequently, FWM causes the most significant spectral broadening near the intensity peak of the pulse, and FRS broadening happens mostly in the pulse tail. This also leads to the *second* distinction that FWM is prominent only with short pulse duration relative to plasma wave periods, and otherwise FRS dominates. *Third*, FRS can only change the frequency of a photon by a single plasma frequency $\pm\omega_p$, but FWM can cause changes in multiple plasma frequencies $\pm j\omega_p$, even for noninteger j's. *Fourth*, FWM creates both a low-frequency photon and a high-frequency photon simultaneously, but FRS creates Stokes or anti-Stokes photons independently. Since the interaction rate is higher for frequency downshift, FRS overall creates more low-frequency photons.

To illustrate the interaction properties of FWM and FRS, we solve Eqs. (7)–(9) numerically and show the results in Fig. 2. We first consider a short Gaussian laser pulse with root-mean-square (rms) duration $T = 2\pi/\omega_p$. The input pulse contains two frequency components at $a_{49} = a_{50} = 0.4e^{-(\zeta/T)^2}$. The double-humped pulse envelope is the result of beating. Their interaction is dominated by FWM in the 250 plasma-wavelength-long plasma. The tempo-spectral diagram in Fig. 2(a) shows that the maximum spectral broadening happens near the peak of the pulse. The output spectrum shown in the top bar plot has a relatively flat distribution with sharp descent at both ends. The side panel shows that the pulse temporal envelope retains its structure despite some slight distortion.

For comparison, we demonstrate an FRS-dominated spectral broadening interaction by increasing the laser pulse duration to $T = 40\pi/\omega_p$. The pulse amplitude is correspondingly reduced to $a_{49} = a_{50} = 0.15e^{-(\zeta/T)^2}$, and the total propagation distance is 800 plasma wavelengths. The plasma wave decay ν is neglected. The output tempo-spectral diagram in Fig. 2(b) shows an increasingly broader spectrum toward the tail of the laser pulse. It forms a grid-like structure with alternating dark and bright spots in both the ζ and ω directions. This indicates that, for a certain frequency component, the pulse is transformed into a series of pulse trains. The time-integrated spectrum, as illustrated in the top bar plot, shows that most of the photons are shifted to lower frequencies. The spectrum has a constant decreasing trend toward both lower- and higher-frequency limits. The temporal envelope retains its modulation structure despite higher peak amplitudes in the pulse tail.

A. Conservation of energy and photon number

The downshift of photon frequencies in the FRS frequency comb indicates a loss of laser energy, which seems to be conserved in the FWM-dominated frequency comb, as shown in Fig. 2. For more rigorous analysis, we quantitatively investigate Eqs. (7)–(9). First, we remind ourselves that the photon energy density in a plasma can be expressed as $\mathcal{E}_{EM} = \{\partial_\omega[\omega\epsilon(\omega)]\epsilon_0 E^2 + B^2/\mu_0\}/2 = \epsilon_0 E^2 \propto \omega^2 a^2$ according to the Landau–Lifshitz formula. The photon number density hence is $\mathcal{E}_{EM}/\omega \propto \omega a^2$. Note that these two expressions have a different form in vacuum. The conservation of total photon number can be obtained exactly from Eq. (7), i.e., $\partial_\tau\left(\int \sum \omega_j |a_j|^2 d\zeta\right) = 0$, where $\omega_j|a_j|^2$ represents the photon number density of the component with frequency ω_j in plasma.

For local photon number density and local laser energy density, we obtain from Eqs. (7)–(9) that

$$\partial_\tau \sum_j \omega_j |a_j|^2 = \partial_\zeta \sum_j \left(1 - \frac{c}{v_{g,j}}\right)\omega_j |a_j|^2, \tag{11}$$

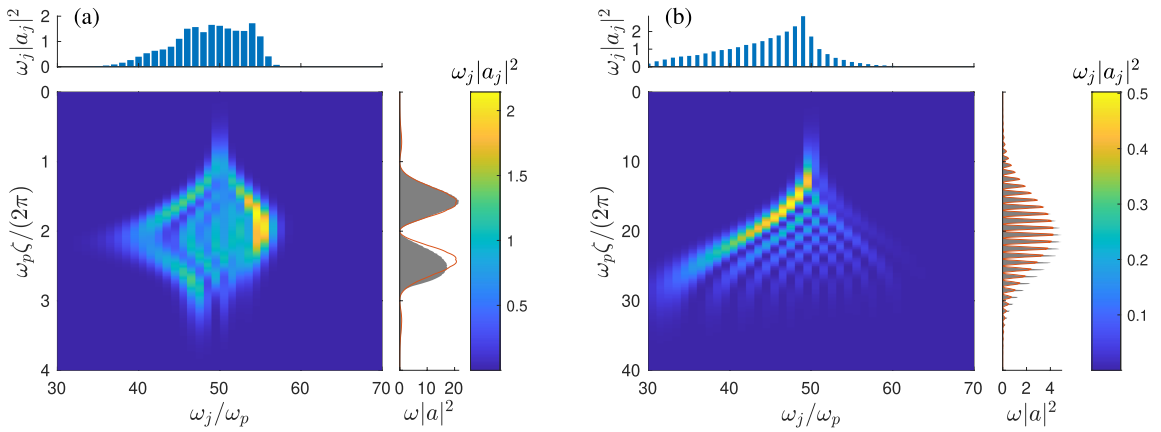

FIG. 2. (a) Tempo-spectral diagram of a short ($T = 2\pi/\omega_p$) laser pulse after propagation in plasma for 250 plasma wavelengths. The initial pulse includes components $a_{49} = a_{50} = 0.4e^{-(\zeta/T)^2}$. (b) Tempo-spectral diagram of the output of a long ($T = 40\pi/\omega_p$) laser pulse after propagation in plasma for 800 plasma wavelengths. The initial pulse includes components $a_{49} = a_{50} = 0.15e^{-(\zeta/T)^2}$. Note the difference in the vertical axis scales. The top panels show the spectral histograms for the whole pulse. The side panels show the temporal envelopes of the initial pulse (red curves) and the final pulse (gray shades). Their full-size envelope plots are shown in Figs. 5 and 6, respectively.

$$\partial_\tau \sum_j \omega_j^2 |a_j|^2 = \partial_\zeta \sum_j \left(1 - \frac{c}{v_{g,j}}\right) \omega_j^2 |a_j|^2 - \omega_p^2 \partial_\zeta |\delta n|^2. \quad (12)$$

We see that the photon number density changes only as a result of group velocity dispersion (GVD), but the laser energy density is affected by both GVD and FRS. Equation (12) has the form $\partial_\tau \mathcal{E}_{\rm EM} = (1/c)\partial_\zeta \mathcal{S}$, which describes the convection of local laser energy $\mathcal{E}_{\rm EM} = \partial_\tau \sum_j \omega_j |a_j|^2$ out of the local region by GVD and by conversion into plasma waves. By integrating over the laser pulse duration from $\zeta = 0$ to ζ_f, we find that the laser energy dissipation rate $\partial_\tau \int_0^{\zeta_f} \mathcal{E}_{\rm EM}\, d\zeta = \omega_p^2 |\delta n(\zeta_f)|^2$ is exactly the plasma wave energy density at the pulse tail. Although the plasma wave transports energy toward the tail of the laser pulse, FRS does not lead to spreading of photon number density, as shown in Eq. (11).

Remarkably, the parametric phase modulation and FWM nonlinearities do not play a role in either photon number density redistribution or laser energy density dissipation. They only contribute to the spectral broadening by affecting the optical refractive index of local plasmas: the plasma electrons are driven to near-relativistic speed by the strong laser field and begin to oscillate in an anharmonic manner. The anharmonicity induces optical nonlinear interaction among different laser frequency components. This parametric nonlinear process does not induce any growing plasma density perturbation or electrostatic fields, and hence does not cause laser energy dissipation. But it does change the plasma dispersion relation and induces a phase change of local photons. In other words, FWM induces virtual phonons and FRS induces real phonons.

B. FRS and growth of plasma waves

Broadening of the laser spectrum is mediated by phonons and virtual phonons of finite amplitude. With a multicolor input laser, the virtual phonon amplitude becomes nonzero instantaneously, but the phonon amplitude grows gradually. To analyze their growth, we separate the different regimes of interaction according to pulse duration.

For pulses with duration longer than a plasma wavelength, FRS dominates. We neglect the FWM interaction and find after combining Eqs. (7) and (8) that

$$(\partial_\zeta - i\nu)\partial_\tau \delta n = \partial_\zeta \sum_j \left(2 - \frac{c}{v_{g,j}} - \frac{c}{v_{g,j+1}}\right) a_j^* a_{j+1} + \frac{\omega_p^3}{4} \sum_j \left(\frac{1}{\omega_{j-1}} - \frac{1}{\omega_{j+1}}\right) |a_j|^2 \delta n. \quad (13)$$

The two terms on the right-hand side describe the effect of GVD and the growth of the plasma wave, respectively. With plasma decay neglected, the second term indicates that the growth of plasma waves is caused by asymmetric interaction rates of phonon absorption and phonon creation: each laser photon a_j can emit a phonon by converting itself into a Stokes photon or absorb a phonon by converting itself into an anti-Stokes photon. Since the coupling strength is larger for lower-frequency components ($\omega_{j-1}^{-1} > \omega_{j+1}^{-1}$), a photon is more likely to be downconverted and create a phonon. The increased phonon number, in turn, enhances the photon–photon interaction.

To find the growth rate, we neglect GVD and write

$$\partial_{\zeta\tau} \delta n = \frac{\omega_p^3}{4} \sum_j (\omega_{j-1}^{-1} - \omega_{j+1}^{-1}) |a_j|^2 \delta n \approx \sum_j \frac{\omega_p^4}{\omega_j^2} \frac{|a_j|^2 \delta n}{2}. \quad (14)$$

Since the created plasma wave does not propagate, we neglect its spatial dynamics, i.e., $\partial_{tt}\delta n \approx \partial_{\zeta\tau}\delta n$. Therefore, the plasma wave growth rate in the long-pulse limit is $\Gamma_{\rm FRS,4} \cong (\omega_p^2/\sqrt{2})\left(\sum_j |a_j|^2/\omega_j^2\right)^{1/2}$,

assuming $\nu \to 0$. It can be reduced to $\omega_p^2 a_0/(\sqrt{2}\,\omega_0)$ in the case of a monochromatic pump. This agrees with Refs. 7–9, apart from a factor of two difference owing to the definition of a_j in Eq. (3). The phonon peak amplitude is located at $\zeta = \tau/2$, i.e., $z = ct/2$. For laser pulses with a short duration T, the plasma wave grows exponentially only for a finite time T. The plasma wave amplitude reaches its maximum amplitude at a distance ζ and grows as $\exp(\Gamma_{\mathrm{FRS},4}\sqrt{\tau\zeta})$, which is shown in Fig. 3.

For high plasma density ($\omega_{j-1}^{-1} \gg \omega_{j+1}^{-1}$), the laser's interaction with its anti-Stokes wave becomes negligible compared with its interaction with its Stokes wave. The phonon dynamics can then be simply described by

$$\partial_{tt}\delta n \approx \partial_{\zeta\tau}\delta n = \frac{\omega_p^3}{\omega_0 - \omega_p}\frac{|a_0|^2\delta n}{4}. \tag{15}$$

Thus, we obtain the "three-wave" FRS growth rate

$$\Gamma_{\mathrm{FRS},3} = \left(\frac{\omega_p^3}{\omega_0 - \omega_p}\right)^{1/2}\frac{a_0}{2}. \tag{16}$$

Since the "three-wave" coupling does not consider the generation of the anti-Stokes wave that absorbs phonons, $\Gamma_{\mathrm{FRS},3}$ is larger than the "four-wave" FRS growth rate $\Gamma_{\mathrm{FRS},4}$.

When a phonon interacts with a photon a_j, whether the scattering creates an anti-Stokes photon a_{j+1} or a Stokes photon a_{j-1} depends on the relative phase of δn and a_j. From Eq. (7), we obtain the photon number dynamics as

$$\left[\partial_\tau + \left(\frac{c}{v_{g,j}} - 1\right)\partial_\zeta\right](\omega_j|a_j|^2) = \mathrm{Re}\left[\omega_p^3(a_{j+1}^*\delta n - a_{j-1}^*\delta n^*)a_j\right] - \mathrm{Im}\left[3\omega_p^2\sum_k a_j a_{j+k}^*\chi_k\right], \tag{17}$$

and $\delta n = \int_0^\zeta \chi_1 e^{-\nu\zeta'}\,\mathrm{d}\zeta'$. On the right-hand side, the first and second terms describe the FRS and FWM interactions, respectively. The FRS interaction can be categorized into resonant terms and non-resonant terms.

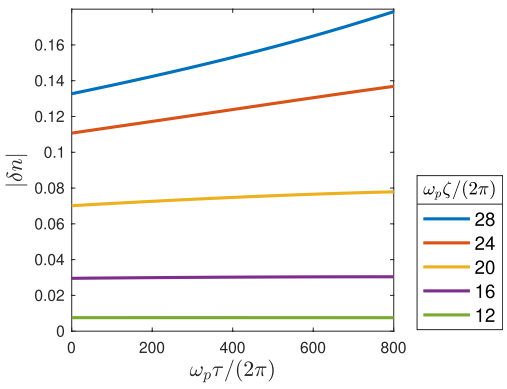

FIG. 3. Plasma wave amplitude at various locations ζ and pulse propagation distances τ. The parameters are the same as in Fig. 2(b).

The resonant photon number growth due to FRS interaction is proportional to $(|a_{j+1}|^2 - |a_{j-1}|^2)|a_j|^2$, with the ζ dependence neglected. On a small time scale, it leads to an exponential growth of the photon number in mode a_j. This amplitude-difference-driven interaction causes a cascade of photon frequency decrease. Starting with a bicolor laser input a_o and a_{o-1}, the resonant FRS interaction initially causes $|a_o|$ to decrease and $|a_{o-1}|$ to increase. A low-frequency mode $|a_{o-2}|$ is created and grows. As $|a_{o-2}|$ approaches and exceeds $|a_o|$, the mode $|a_{o-1}|$ begins to decrease. Without photon supplementation from higher-frequency modes, $|a_o|$ eventually reaches zero amplitude. Overall, modes are created at the low-frequency limit and are annihilated in the high-frequency limit, causing a successive frequency downshift. The trend of downshift can be seen as the bright stream in the main plot of Fig. 2(b). The resonant frequency downshift process asymptotically results in more low-frequency sidebands with monotonically decreasing amplitudes, as can be seen in the top panel of Fig. 2(b).

The nonresonant FRS interaction is described by the terms proportional to

$$Re\left[\left(a_{j+1}^*\int_0^\zeta \chi_1 e^{-\nu\zeta'}\,\mathrm{d}\zeta' - a_{j-1}^*\int_0^\zeta \chi_1^* e^{-\nu\zeta'}\,\mathrm{d}\zeta'\right)a_j\right].$$

Since it is proportional to a_j, the nonresonant FRS has a lower growth rate. The nonresonant FRS can create both frequency-upshifted photons and frequency-downshifted photons, similar to a FWM-type interaction.

C. FWM and evolution of virtual phonons

Laser pulses with a short duration near a plasma wavelength are not sufficient to generate strong plasma waves, and hence FWM dominates. FWM creates new frequency components by scattering the laser photons via virtual phonons. The virtual phonons do not have an eigenfrequency and are totally determined by the beating lasers. Hence, FWM can upshift or downshift a laser photon by multiple times the plasma frequency.

The FWM growth rate depends on the virtual phonon amplitude. With the FRS interaction neglected, the virtual phonon dynamics are obtained by combining Eqs. (7) and (9):

$$\partial_\tau\sum_k|\chi_k|^2 = \sum_{j,k}\chi_k\left(1 - \frac{c}{v_{g,j}}\right)\partial_\zeta(a_j a_{j+k}^* + a_{j-k}a_j^*), \tag{18}$$

$$\partial_\tau(\chi_k \pm \chi_{-k}) = \sum_j\left(1 - \frac{c}{v_{g,j}}\right)\partial_\zeta[a_j(a_{j+k}^* \pm a_{j-k}^*)] + \frac{3\omega_p^2}{4i}\sum_{j,k'}\left(\frac{1}{\omega_j} - \frac{1}{\omega_{j-k-k'}}\right)\chi_{k'}a_{j-k'}a_{j-k}^* \pm \frac{3\omega_p^2}{4i}\sum_{j,k'}\left(\frac{1}{\omega_j} - \frac{1}{\omega_{j+k-k'}}\right)\chi_{k'}a_{j-k'}a_{j+k}^*. \tag{19}$$

Since $\chi_{-k} = \chi_k^*$, Eq. (19) for $\pm$ describes the evolution of the real and imaginary parts of χ_k, respectively. The identity (18) indicates that the total virtual phonon amplitude is conserved when GVD is neglected. Hence, none of the χ_k can grow exponentially. With GVD, the growth of χ_k is driven by other $\chi_{k'}$ ($k' \neq k$) terms, provided that $a_j a_{j-(k-k')}^*$ are nonzero. Since the coefficients $(1/\omega_j - 1/\omega_{j\pm k-k'}) \sim (k' \pm k)/(j\omega_j)$ are small in value, the growth of χ_k is lower than the growth of a_j. Hence,

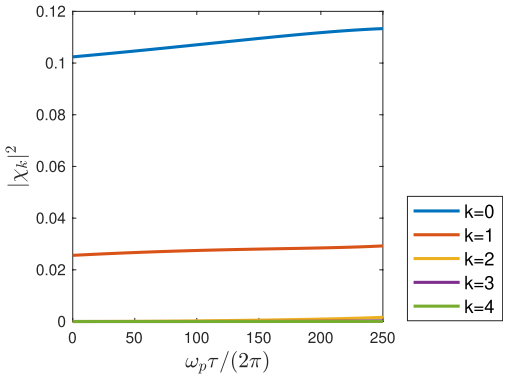

FIG. 4. Amplitudes of virtual phonons $|\chi_k|$ at the pulse peak $\zeta/(c\omega_p) = 1$. The parameters are the same as in Fig. 2(a).

χ_k can be approximated as quasi-constants. The quasi-conservation is numerically verified and illustrated in Fig. 4, which shows only nonzero $\chi_{0,\pm1}$ for the bicolor input laser.

The photon number growth due to FWM is described by the second term on the right-hand side of Eq. (17). Because the imaginary part is taken, it does not include any resonant terms. Thus, the spectrum expands to both lower and higher frequencies equally. In contrast to the FRS interaction, FWM grows fastest at the pulse intensity peak. Thus, the tempo-spectral diagram in Fig. 2(a) shows broad bands only at the peak center.

The dominance of low-order terms $\chi_{0,\pm1}$ in Fig. 4 means that the new laser frequency components are generated at an interval of ω_p. This differs from Ref. 39, in which the aim is to substantially upshift the laser frequency by the injection of two highly detuned pulses with frequency differences greater than the plasma frequency. Similar to Ref. 39, however, both upshift and downshift of the photon frequency coexist in the FWM process we describe here.

IV. SCALING OF FREQUENCY BANDWIDTH GROWTH

With a bicolor laser input, only χ_0 and $\chi_{\pm1}$ are nonzero. For quasi-steady values of χ_k, we can find the analytical solution to the recursion equation in the limit of small bandwidth $\max(\omega_j) - \min(\omega_j) \ll \omega_j$, and hence

$$a_j(\tau,\zeta) = \sum_o a_o(0,\zeta) e^{i(j-o)\left(\frac{\pi}{2}-\psi\right)} \times \exp\left(\frac{3i\omega_p^2\chi_0\tau}{4\omega_j}\right) J_{j-o}\left(\frac{3\omega_p^2|\chi_1|}{2\omega_o}\tau\right), \quad (20)$$

where the o's denote the indices of the input laser fields, and ψ is the phase of χ_1, i.e., $e^{i\psi} = \chi_1/|\chi_1| \cong 1$. The solution shows that each input laser component expands to a broad spectrum whose amplitude is described by the Bessel function J_{j-o}. The contribution from different a_o's differ by a phase of $\pi/2$, and so they do not interfere. The photon number in each mode is then

$$\omega_j|a_j(\tau,\zeta)|^2 \cong \omega_j \sum_o |a_o(0,\zeta)|^2 J_{j-o}^2\left(\frac{3\omega_p^2|\chi_1|}{2\omega_o}\tau\right). \quad (21)$$

Since the first peak of $J_{\pm j}(x)$ is located at approximately $x \sim |j|$, the laser spectral width $\Delta\omega_{\mathrm{FWM}}$ expands with the scaling

$$\Delta\omega_{\mathrm{FWM}} \sim \frac{3\omega_p^2|\chi_1|}{\omega_o}\tau = \frac{3\omega_p^2|a_o a_{o-1}^*|}{\omega_o}\tau. \quad (22)$$

For the parameters used in Fig. 2(a), the output bandwidth reaches $\pm16\omega_p$, which agrees well with the simulation results.

Equation (20) has a similar form to the solution for the FRS interaction found by Karttunen and Salomaa[26,27] augmented with a self-phase modulation term. For the FRS interaction, Eq. (20) should be modified by replacing $e^{i\psi} = \delta n/|\delta n| \cong i$ and $|\chi_1|/ \to |\delta n|$:

$$a_j(\tau,\zeta) \simeq \sum_o a_o(0,\zeta)(-1)^{j-o} J_{j-o}\left(\frac{\omega_p^2|\delta n|}{\omega_o}\tau\right), \quad (23)$$

The change in ψ causes a π phase difference between the spectra from different a_o's. Using the identity $J_{-j}(\cdot) = (-1)^j J_j(\cdot)$, we obtain the following estimate of the photon number:

$$\omega_j|a_j(\tau,\zeta)|^2 \simeq \omega_j\left[\sum_o (\mp1)^o |a_o(0,\zeta)| J_{j-o}\left(\frac{\omega_p^2|\delta n|}{\omega_o}\tau\right)\right]^2, \quad (24)$$

where $\mp$ are for positive and negative values of $j - o$, respectively. Thus, the spectral broadening to the high-frequency band is suppressed owing to destructive interference, and the spectral expansion to the lower-frequency bands is enhanced owing to constructive interference, as can be seen from Fig. 2(b). Since the spectral broadening is only to the lower-frequency bands, the scaling is

$$\Delta\omega_{\mathrm{FRS}} \sim \frac{\omega_p^2|\delta n|}{\omega_o}\tau = \frac{\omega_p^3\tau}{2\omega_o}\left|\int_0^\zeta a_o a_{o-1}^* e^{-\nu\zeta'}\,\mathrm{d}\zeta'\right|. \quad (25)$$

For the parameters used in Fig. 2(a), the output spectrum extends to lower frequencies by $\pm15\omega_p$, which agrees in order of magnitude with the simulation results. It should be born in mind that the solution only approximately describes the spectral evolution, because the plasma amplitude δn changes, as we can see from Fig. 3.

Comparing Eqs. (22) and (25), we find that the spectral bandwidth broadenings due to FWM or FRS have the same dependence on the parameters, including the interaction time τ and input frequency ω_o. They both increase with higher pump amplitude multiplication $\chi_1(0,\zeta) = a_o(0,\zeta)a_{o-1}(0,\zeta)$, but FWM grows proportionally to $|\chi_1(0,\zeta)|$ and FRS depends on its integral $\left|\int_0^\zeta \chi_1(0,\zeta')e^{-\nu\zeta'}\,\mathrm{d}\zeta'\right|$. Therefore, FWM dominates when the pulse duration is as short as a few plasma wavelengths, and it broadens the laser spectrum most significantly at the pulse intensity peak, whereas FRS dominates with longer pulse duration, and it broadens the laser spectrum most significantly at the pulse tail.

V. PULSE ENVELOPE MODULATION

A larger laser spectral bandwidth $\Delta\omega$, in principle, supports shorter laser pulses, provided that all the frequency components interfere constructively with identical phase. However, Eqs. (20) and (23) show that the frequency comb components both have opposite phases at different j's. This phase flipping prevents the pulse from forming sharp peaks.

Actually, we can find the analytical solution to the pulse temporal envelope in the limit of large spectral width. Note the generating

function of the Bessel function, $e^{ix\cos(\phi)} = \sum_{j=-\infty}^{+\infty} i^j J_j(x) e^{ij\phi}$. For the FWM interaction, the laser field a can be found by combining Eqs. (3) and (20) and using $\omega_j - \omega_o = (j-o)\omega_p$:

$$\begin{aligned} a &= 2\mathrm{Re}\sum_{o,j} a_o(0,\zeta) i^{j-o} \exp\left(\frac{3i\omega_p^2\chi_0\tau}{4\omega_j}\right) J_{j-o}\left(\frac{3\omega_p^2|\chi_1|}{2\omega_o}\tau\right) e^{-i\omega_j\zeta} \\ &\approx 2\mathrm{Re}\sum_{o} a_o(0,\zeta) \exp\left[\frac{3i\omega_p^2\chi_0\tau}{4\omega_o} + i\frac{3\omega_p^2|\chi_1|}{2\omega_o}\tau\cos(\omega_p\zeta) + i\omega_o\zeta\right] \\ &= \sum_{o} a_o(0,\zeta)\cos\left[\frac{3\omega_p^2\chi_0}{4\omega_j}\tau + \frac{3\omega_p^2|\chi_1|}{2\omega_o}\tau\cos(\omega_p\zeta) + \omega_o\zeta\right]. \end{aligned} \tag{26}$$

This result shows that each pump pulse a_o is frequency-modulated by the FWM interaction: the χ_0 term describes the phase modulation, which induces a chirp proportional to $\partial_\zeta\chi_0(\tau,\zeta)\tau = \partial_\zeta\left|\sum_o a_o(0,\zeta)\right|^2\tau$, while the χ_1 term creates new sidebands and modulates the envelope at frequency ω_p. The frequency modulation index $\Delta\omega_{\mathrm{FWM}}/2 = \omega_p|\chi_1|\tau/(\omega_o)$ grows linearly with τ. The increasing modulation index due to FWM broadens the laser spectrum, thereby allowing pulse duration compression.

For FWM-dominated spectral broadening, the pump pulse duration is shorter than a few plasma wavelengths. The frequency modulation thus causes a frequency chirp near the pulse center ζ_M. Owing to the strong ζ dependence of $\chi_0(\tau,\zeta) \simeq \sum_o |a_o(0,\zeta)|^2$, the phase modulation enhances the frequency chirp by causing increasingly higher frequency upshift toward the tail. On the other hand, since higher-frequency components propagate faster in a plasma, GVD causes negative chirp. If the chirping due to FWM and GVD is balanced, the laser pulse duration is then compressed and the peak amplitude is enhanced. Such a principle is adopted in Refs. 29 and 30 to obtain few-cycle laser spikes.

Figure 5 zooms in on the side panel of Fig. 2(a) and shows the frequency chirp. The filled area represents the fast oscillating pulse envelope at $2\pi/(50\omega_p)$. Note that the double-hump structure of the input pulse arises from beating of the two frequency components. The pulse envelope maintains the same structure. The output pulse obviously develops a negative-frequency chirp indicating the dominant role of GVD. The nearly linearly chirped peaks could then be compressed into two sharp and intense peaks through proper dispersion management.

For FRS interaction, the laser field can be found similarly by combining Eqs. (3) and (23):

$$\begin{aligned} a &\simeq 2\mathrm{Re}\sum_{o,j} a_o(0,\zeta)(-1)^{j-o} J_{j-o}\left(\frac{\omega_p^2|\delta n|}{\omega_o}\tau\right) e^{-i\omega_j\zeta} \\ &\approx 2\mathrm{Re}\sum_{o} a_o(0,\zeta)\exp\left[i\left(\frac{\omega_p^2|\delta n|}{\omega_o}\tau\right)\sin(\omega_p\zeta) + \omega_o\zeta\right] \\ &= \sum_{o} a_o(0,\zeta)\cos\left[\left(\frac{\omega_p^2|\delta n|}{\omega_o}\tau\right)\sin(\omega_p\zeta) + \omega_o\zeta\right]. \end{aligned} \tag{27}$$

This result shows that FRS causes frequency modulation of the laser pulse with increasing modulation index, similarly to FWM. The broadened spectrum, combined with GVD, compresses the pulse duration and increases the peak amplitude.

Figure 6 zooms in on the side panel of Fig. 2(b) and shows the instantaneous frequency within the pulse. The isolated peak structure with a period of $2\pi/\omega_p$ is the result of beating between two pumps at $49\omega_p$ and $50\omega_p$. The plot exhibits the greatest changes in the pulse envelope in the peak and tail of the pulse, where the plasma wave is the strongest. Because chirps are developed individually within each

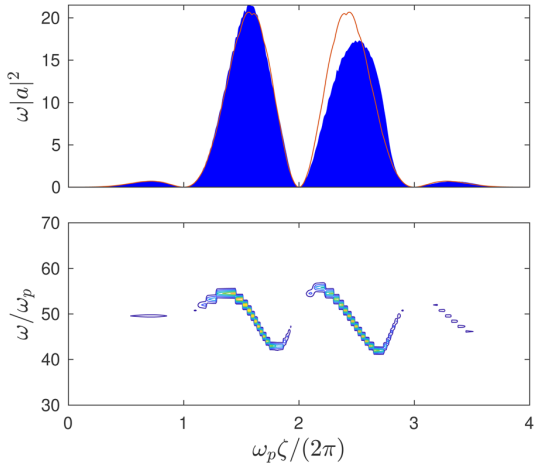

FIG. 5. (a) Input (red curve) and output (blue shade) pulse envelopes of a short laser pulse $T = 2\pi/\omega_p$. (b) Contour plot of the time–frequency synchrosqueezed transform. The parameters are the same as in Fig. 2(a).

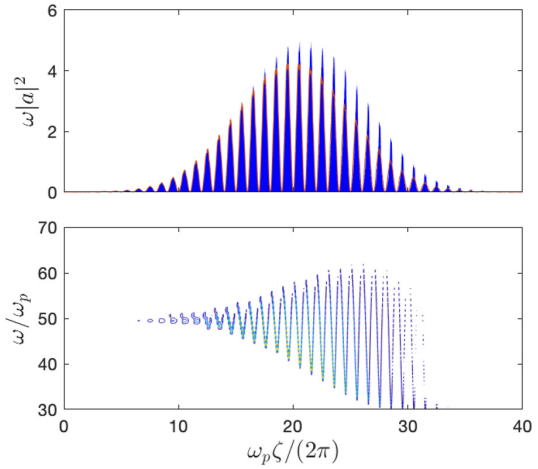

FIG. 6. (a) Input (red curve) and output (blue shade) pulse envelopes of a short laser pulse $T = 40\pi/\omega_p$. (b) Contour plot of the time–frequency synchrosqueezed transform. The parameters are the same as in Fig. 2(b).

spike, the pulse train cannot be compressed into a single pulse to increase its peak intensity.

VI. PIC SIMULATIONS

As a proof-of-principle demonstration of the generation of a supercontinuum and frequency comb, we conduct PIC simulations using the fully relativistic kinetic code EPOCH.[45] The input laser pulse in each simulation comprises two frequency components with wavelengths 1 and 0.98 μm, respectively. They both have a Gaussian profile, i.e., $a = \sum_o a_o \exp[-\frac{1}{2}(\zeta/T)^2 + i\omega_o t]$, and their beating causes a multiple-peak structure. The uniform plasma has a density of 4.47×10^{17} cm^{-3}, corresponding to a plasma frequency 1/50 of the 1 μm laser. Hence, the plasma wavelength is $\lambda_p = 2\pi/k_p = 50$ μm. The output laser pulses after propagating through the 40-mm-long plasma ($800\lambda_p$) are shown in Fig. 7.

Figures 7(a) and 7(c) show frequency broadening of a short and intense pulse into a supercontinuum. Each input pulse component has duration $T = 0.15$ ps (0.9 plasma period) and peak amplitude $a_o = 0.4$ (corresponding to $I = 2.2 \times 10^{17}$ W cm^{-2}). The output pulse envelope shows some degree of compression in the tail. We take the Fourier transform of the laser electric field at the snapshot to obtain its wavevector spectrum. The spectrum in Fig. 7(c) shows a supercontinuum with bandwidth ~$0.8\omega_o$.

Figures 7(b) and 7(d) show frequency broadening of a long and less intense pulse into a frequency comb. Each input pulse component has duration $T = 1.5$ ps (nine plasma periods) and peak amplitude $a_o = 0.12$ (corresponding to $I = 2 \times 10^{16}$ W cm^{-2}). The output envelope shows a small amount of pulse compression in the tail of the pulse. Fourier transformation of its electric field yields a frequency comb with discrete equidistant spikes spanning from below $20k_p$ to $70k_p$. The result agrees well with our analysis, which justifies the use of Eqs. (1) and (2).

VII. CONCLUSION AND DISCUSSION

We have shown that a laser pulse can be expanded into a broadband spectrum when propagating through a tenuous plasma. This spectral broadening arises from a cascade of both Stokes and anti-Stokes scattering due to plasma waves and electron relativistic effects. We point out that a few-cycle pulse with near-relativistic intensity can produce an octave-wide supercontinuum through FWM and phase modulation, and a multicycle pulse can produce an octave-wide frequency comb through FRS. As the frequency comb bandwidth increases, it continues to lose energy to the plasma wave. As a result, the lower-frequency components grow faster than the higher-frequency ones, and the comb loses total laser energy. The comb expands to lower frequencies. But the supercontinuum conserves laser energy because the amplitudes of virtual phonons do not change. Hence, the supercontinuum spectrum broadens symmetrically to both lower and higher frequencies. It should be mentioned that a similar FWM process has been investigated in Ref. 39 with the aim of achieving resonant laser frequency doubling by arranging the frequencies and intensities of two highly detuned lasers. The present article has focused on a different regime in which both FRS and FWM processes broaden the input laser spectrum by a multiple integer times the plasma frequency.

Compared with the use of optical crystals for generating optical supercontinuum and frequency combs, plasmas have high thermal damage tolerance and can work in the near-relativistic regime. Ultraintense broadband pulses are particularly useful for minimizing laser scattering and absorption in laser–plasma applications such as inertial confinement fusion and laser–plasma accelerators. Using plasmas, the supercontinua or frequency combs can be generated in the EUV or x-ray regions. The equidistant peaks of the frequency comb could also enable potential applications in ultrafast optics at ultra-high intensities, for example, for creating high-intensity terahertz waves.

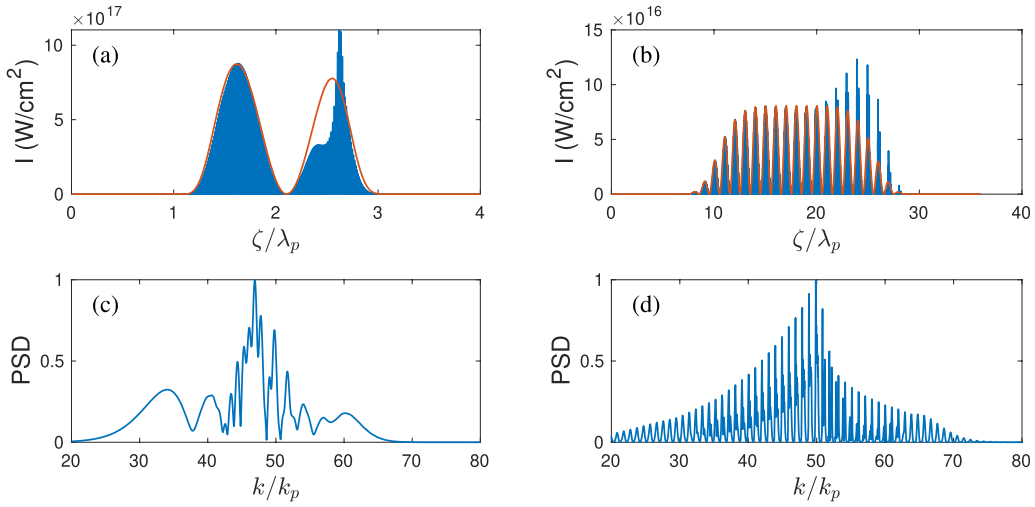

FIG. 7. PIC simulation results for a supercontinuum [(a) and (c)] generated from a short laser pulse in the FWM-dominated regime, and a frequency comb [(b) and (d)] generated from a long laser pulse in the FRS-dominated regime. In (a) and (b), the red curves show the initial pulse envelope, and the blue shade shows the output signal. (c) and (d) show the power spectral density (PSD) of the corresponding output signals.

The experimental feasibility of this method has been demonstrated through PIC simulations of a frequency comb using accessible parameters. The parameters of laser wavelength, peak intensity, and plasma length are similar to those in laser particle accelerators,[19] but the requirements are less stringent for generation of a supercontinuum or frequency comb. The peak laser intensity of 10^{16}–10^{17} W cm^{-2} is sufficient to enter the mildly relativistic regime. It can pass through a few-centimeter-long plasma with density 10^{17}–10^{18} cm^{-3}. At such a low density, collisional plasma damping can be neglected, and the consequent low plasma wavenumber (which is proportional to ω_p/ω_0) also avoids Landau damping.

The proposed method for generating frequency combs does not rely on an optical resonator, as is required for conventional methods using, for example, a mode-locked laser. Since the laser spectrum is broadened after a single pass through the plasma, the comb quality is limited by plasma inhomogeneity. Specifically, short-range plasma density inhomogeneities destroy the FRS resonance, reducing the efficiency of frequency band broadening. More seriously, the long-range plasma density inhomogeneity could gradually shift the FRS resonance, resulting in fluctuations of the comb repetition rate. Plasma inhomogeneity, however, does not affect the generation of the supercontinuum, which does not depend on resonance with the plasma frequency.

Our analysis applies to 1D propagation of lasers with below-relativistic intensity and pulse duration not too much shorter than a plasma wavelength. For ultrarelativistic laser intensity, the laser–plasma interaction becomes fully nonlinear[46,47] and our theory is no longer valid. A pulse duration much shorter than a plasma wavelength produces a strong wakefield,[19] which can significantly alter the evolution of the laser envelope. To avoid pulse distortion in long plasmas, the laser power needs to be below the critical power for transverse filamentation.[5,6]

ACKNOWLEDGMENTS

This work was supported by NNSA Grant No. DE-NA0002948.

REFERENCES

[1]J. J. Thomson and J. I. Karush, "Effects of finite-bandwidth driver on the parametric instability," Phys. Fluids **17**, 1608–1613 (1974).
[2]A. N. Mostovych, S. P. Obenschain, J. H. Gardner, J. Grun, K. J. Kearney, C. K. Manka, E. A. McLean, and C. J. Pawley, "Brillouin scattering measurements from plasmas irradiated with spatially and temporally incoherent laser light," Phys. Rev. Lett. **59**, 1193–1196 (1987).
[3]J. A. Marozas, M. Hohenberger, M. J. Rosenberg, D. Turnbull, T. J. B. Collins, P. B. Radha, P. W. McKenty, J. D. Zuegel, F. J. Marshall, S. P. Regan, T. C. Sangster, W. Seka, E. M. Campbell, V. N. Goncharov, M. W. Bowers, J.-M. G. Di Nicola, G. Erbert, B. J. MacGowan, L. J. Pelz, and S. T. Yang, "First observation of cross-beam energy transfer mitigation for direct-drive inertial confinement fusion implosions using wavelength detuning at the national ignition facility," Phys. Rev. Lett. **120**, 085001 (2018).
[4]C. J. McKinstrie and R. Bingham, "Stimulated Raman forward scattering and the relativistic modulational instability of light waves in rarefied plasma," Phys. Fluids B **4**, 2626 (1992).
[5]T. M. Antonsen and P. Mora, "Self-focusing and Raman scattering of laser pulses in tenuous plasmas," Phys. Rev. Lett. **69**, 2204 (1992).
[6]T. M. Antonsen and P. Mora, "Self-focusing and Raman scattering of laser pulses in tenuous plasmas," Phys. Fluids B **5**, 1440 (1993).
[7]W. B. Mori, C. D. Decker, D. E. Hinkel, and T. Katsouleas, "Raman forward scattering of short-pulse high-intensity lasers," Phys. Rev. Lett. **72**, 1482–1485 (1994).
[8]C. D. Decker, W. B. Mori, K.-C. Tzeng, and T. Katsouleas, "The evolution of ultra-intense, short-pulse lasers in underdense plasmas," Phys. Plasmas **3**, 2047 (1996).
[9]C. D. Decker, W. B. Mori, T. Katsouleas, and D. E. Hinkel, "Spatial temporal theory of Raman forward scattering," Phys. Plasmas **3**, 1360 (1996).
[10]K. V. Lezhnin, K. Qu, and N. J. Fisch, "Suppression of power losses during laser pulse propagation in underdense plasma slab," Phys. Plasmas **28**, 023112 (2021).
[11]M. R. Edwards, K. Qu, J. M. Mikhailova, and N. J. Fisch, "Beam cleaning of an incoherent laser via plasma Raman amplification," Phys. Plasmas **24**, 103110 (2017).
[12]Y. Zhao, S. Weng, M. Chen, J. Zheng, H. Zhuo, C. Ren, Z. Sheng, and J. Zhang, "Effective suppression of parametric instabilities with decoupled broadband lasers in plasma," Phys. Plasmas **24**, 112102 (2017).
[13]J. P. Palastro, J. G. Shaw, R. K. Follett, A. Colaïtis, D. Turnbull, A. V. Maximov, V. N. Goncharov, and D. H. Froula, "Resonance absorption of a broadband laser pulse," Phys. Plasmas **25**, 123104 (2018).
[14]A. A. Solodov, V. M. Malkin, and N. J. Fisch, "Random density inhomogeneities and focusability of the output pulses for plasma-based powerful backward Raman amplifiers," Phys. Plasmas **10**, 2540–2544 (2003).
[15]S. Y. Kalmykov, S. A. Yi, and G. Shvets, "All-optical suppression of relativistic self-focusing of laser beams in plasmas," Phys. Rev. E **78**, 057401 (2008).
[16]S. Kalmykov, S. Austin Yi, and G. Shvets, "All-optical control of nonlinear focusing of laser beams in plasma beat wave accelerator," Plasma Phys. Controlled Fusion **51**, 024011 (2009).
[17]K.-C. Tzeng, W. B. Mori, and C. D. Decker, "Anomalous absorption and scattering of short-pulse high-intensity lasers in underdense plasmas," Phys. Rev. Lett. **76**, 3332–3335 (1996).
[18]R. K. Follett, J. G. Shaw, J. F. Myatt, J. P. Palastro, R. W. Short, and D. H. Froula, "Suppressing two-plasmon decay with laser frequency detuning," Phys. Rev. Lett. **120**, 135005 (2018).
[19]E. Esarey, C. B. Schroeder, and W. P. Leemans, "Physics of laser-driven plasma-based electron accelerators," Rev. Mod. Phys. **81**, 1229 (2009).
[20]R. S. Craxton, K. S. Anderson, T. R. Boehly, V. N. Goncharov, D. R. Harding, J. P. Knauer, R. L. McCrory, P. W. McKenty, D. D. Meyerhofer, J. F. Myatt, A. J. Schmitt, J. D. Sethian, R. W. Short, S. Skupsky, W. Theobald, W. L. Kruer, K. Tanaka, R. Betti, T. J. B. Collins, J. A. Delettrez, S. X. Hu, J. A. Marozas, A. V. Maximov, D. T. Michel, P. B. Radha, S. P. Regan, T. C. Sangster, W. Seka, A. A. Solodov, J. M. Soures, C. Stoeckl, and J. D. Zuegel, "Direct-drive inertial confinement fusion: A review," Phys. Plasmas **22**, 110501 (2015).
[21]S. Corde, K. Ta Phuoc, G. Lambert, R. Fitour, V. Malka, A. Rousse, A. Beck, and E. Lefebvre, "Femtosecond x rays from laser-plasma accelerators," Rev. Mod. Phys. **85**, 1–48 (2013).
[22]W. Koechner, "Thermal lensing in a Nd:YAG laser rod," Appl. Opt. **9**, 2548–2553 (1970).
[23]B. C. Stuart, M. D. Feit, A. M. Rubenchik, B. W. Shore, and M. D. Perry, "Laser-induced damage in dielectrics with nanosecond to subpicosecond pulses," Phys. Rev. Lett. **74**, 2248–2251 (1995).
[24]B. I. Cohen, A. N. Kaufman, and K. M. Watson, "Beat heating of a plasma," Phys. Rev. Lett. **29**, 581 (1972).
[25]M. N. Rosenbluth and C. S. Liu, "Excitation of plasma waves by two laser beams," Phys. Rev. Lett. **29**, 701–705 (1972).
[26]R. R. E. Salomaa and S. J. Karttunen, "Application and generation of large amplitude plasma waves by beating of two intense laser beams," Phys. Scr. **33**, 370 (1986).
[27]S. J. Karttunen and R. R. E. Salomaa, "Electromagnetic field cascading in the beat-wave generation of plasma waves," Phys. Rev. Lett. **56**, 604 (1986).
[28]P. Gibbon, "The self-trapping of light waves by beat-wave excitation," Phys. Fluids B **2**, 2196–2208 (1990).
[29]S. Kalmykov and G. Shvets, "Compression of laser radiation in plasmas using electromagnetic cascading," Phys. Rev. Lett. **94**, 235001 (2005).
[30]S. Kalmykov and G. Shvets, "Nonlinear evolution of the plasma beat wave: Compressing the laser beat notes via electromagnetic cascading," Phys. Rev. E **73**, 046403 (2006).
[31]S. T. Cundiff and J. Ye, "*Colloquium*: Femtosecond optical frequency combs," Rev. Mod. Phys. **75**, 325–342 (2003).

[32]T. M. Fortier, P. A. Roos, D. J. Jones, S. T. Cundiff, R. D. R. Bhat, and J. E. Sipe, "Carrier-envelope phase-controlled quantum interference of injected photocurrents in semiconductors," Phys. Rev. Lett. **92**, 147403 (2004).

[33]T. Udem, R. Holzwarth, and T. W. Hänsch, "Optical frequency metrology," Nature **416**, 233–237 (2002).

[34]T. Fortier and E. Baumann, "20 years of developments in optical frequency comb technology and applications," Commun. Phys. **2**, 153 (2019).

[35]L.-L. Yu, Y. Zhao, L.-J. Qian, M. Chen, S.-M. Weng, Z.-M. Sheng, D. A. Jaroszynski, W. B. Mori, and J. Zhang, "Plasma optical modulators for intense lasers," Nat. Commun. **7**, 11893 (2016).

[36]D. G. Steel and J. F. Lam, "Degenerate four-wave mixing in plasmas," Opt. Lett. **4**, 363–365 (1979).

[37]J. F. Federici, "Review of four-wave mixing and phase conjugation in plasmas," IEEE Trans. Plasma Sci. **19**, 549–564 (1991).

[38]V. M. Malkin and N. J. Fisch, "Towards megajoule x-ray lasers via relativistic four-photon cascade in plasma," Phys. Rev. E **101**, 023211 (2020).

[39]V. M. Malkin and N. J. Fisch, "Resonant four-photon scattering of collinear laser pulses in plasma," Phys. Rev. E **102**, 063207 (2020).

[40]J. M. Dudley, G. Genty, and S. Coen, "Supercontinuum generation in photonic crystal fiber," Rev. Mod. Phys. **78**, 1135–1184 (2006).

[41]J. M. Dudley and G. Genty, "Supercontinuum light," Phys. Today **66**(7), 29–34 (2013).

[42]J. M. Dawson, "Nonlinear electron oscillations in a cold plasma," Phys. Rev. **113**, 383 (1959).

[43]C. J. McKinstrie, A. Simon, and E. A. Williams, "Nonlinear saturation of stimulated Raman scattering in a homogeneous plasma," Phys. Fluids **27**, 2738 (1984).

[44]A. A. Balakin, G. M. Fraiman, Q. Jia, and N. J. Fisch, "Influence of nonlinear detuning at plasma wavebreaking threshold on backward Raman compression of non-relativistic laser pulses," Phys. Plasmas **25**, 063106 (2018).

[45]T. D. Arber, K. Bennett, C. S. Brady, A. Lawrence-Douglas, M. G. Ramsay, N. J. Sircombe, P. Gillies, R. G. Evans, H. Schmitz, A. R. Bell, and C. P. Ridgers, "Contemporary particle-in-cell approach to laser-plasma modelling," Plasma Phys. Controlled Fusion **57**, 113001 (2015).

[46]P. Sprangle, E. Esarey, and A. Ting, "Nonlinear theory of intense laser-plasma interactions," Phys. Rev. Lett. **64**, 2011–2014 (1990).

[47]P. Sprangle, E. Esarey, and A. Ting, "Nonlinear interaction of intense laser pulses in plasmas," Phys. Rev. A **41**, 4463–4469 (1990).